Performance Evaluation of High Dynamic Range Image Tone Mapping Operators Based on Separable Non-linear Multiresolution Families

Ba Chien Thai *, Anissa Mokraoui* and Basarab Matei†
*L2TI,†LIPN, Institut Galilée, Université Paris 13 Sorbonne Paris Cité
99 avenue Jean-Baptiste Clément 93430 Villetaneuse, France
{bachien.thai, anissa.mokraoui}@univ-paris13.fr, matei@lipn.univ-paris13.fr

***Abstract*—This paper addresses the conversion problem of High Dynamic Range (HDR) images into Low Dynamic Range (LDR) images. In this objective, separable non-linear multiresolution approaches are exploited as Image Tone Mapping Operators (TMOs). They are related on: (i) Essentially Non-Oscillatory (ENO) interpolation strategy developed by Harten namely Point-Value (PV) multiresolution family and Cell-Average (CA) multiresolution family; and (ii) Power-P multiresolution family introduced by Amat. These approaches have the advantage to take into account the singularities, such as edge points of the image, in the mathematical model thus preserving the structural information of the HDR images. Moreover the Gibbs phenomenon, harmful in tone mapped images, is avoided. The quality assessment of the tone mapped images is measured according to the TMQI metric. Simulation results show that the proposed TMOs provide good results compared to traditional TMO strategies.**

***Index Terms*—High dynamic range, Tone mapping, Essentially non-oscillatory interpolation, Non-linear multiresolution, Point-value and cell-average multiresolution, Power-P multiresolution.**

1. Introduction

The Human Visual System (HVS) is able to perceive real-word scenes with a wide range of colors and intensities. To be faithful to the HVS, the real-world scene acquisition consists in capturing multiple Low Dynamic Range (LDR) images with different levels of exposure of the scene. These images are then merged building an image as faithful as the real-world scene where its very dark and bright areas are rendered at the same time. Such images, with excellent visual quality, are known as High Dynamic Range (HDR) images avoiding under and over exposure areas that can be perceived on LDR images. However these HDR images cannot be visualized on standard LDR display devices since their dynamic range is smaller than that of HDR images. Moreover HDR display devices currently remain too expensive. Therefore many image Tone Mapping Operators (TMOs) have been proposed [1]. Their main concerns is to reduce the dynamic range (contrast, color gamut, details...) of HDR images to the dynamic range of LDR display device while preserving the appearance of the captured scene in terms of contrast and the overall impression of brightness and colors.

Since these recent years a huge number of research studies on image TMO topic have been developed. Although each TMO approach has its own underlying strategy, it is not possible to review all the developed work in this paper. However a state of the art is fairly complete in reference [1] where a TMO classification into local operators, global operators, segmentation operators, frequency operators and perceptual operators is proposed.

In what follows, we briefly present only some selected TMOs that will be used to evaluate the performance of our approach. In [2], Durand and Dorsey proposed a TMO reducing the HDR contrast while preserving the image details. This work uses an edge-preserving bilateral filter to decompose the HDR image into two layers: a base layer encoding large-scale variations and a detail one. Contrast is then reduced only in the first layer while the details are kept unchanged. The combination of these TM layers produce the LDR image. The TMO is performed on the logarithmic domain, considering that the difference between the logarithmic pixel intensities can refer to a contrast measure. In [3], Drago et al. presented an adaptive logarithmic mapping method of luminance values. It concerns the adaptive adjustment of the logarithmic basis depending on the radiance of the pixels. A set of logarithmic functions ranging from $\log 2$ to $\log 10$ were used to preserve scene details and to improve the rendering contrast. A bias power function was used to ensure a smooth interpolation between the different logarithm bases. In [6], Li et al. proposed a subband architecture related on an oversampled Haar pyramid representation. Subband coefficients are re-scaled using a gain control function reducing the high frequency magnitudes and boosting low ones. The modified subbands are then convolved with the Haar synthesis filters and summed to reconstruct the final LDR image. In [7], Duan et al. proposed an optimization approach based on a histogram adjustment between linear mapping and equalized histogram mapping. In [8], Fattal et al. proposed a second generation of wavelets based on the edge content of the image avoiding having pixels from both sides of an edge. This approach was then exploited to map an HDR image into an LDR image.

This paper evaluates the performance of TMOs related

978-0-9928-6265-7/16/$31.00 ©2016 IEEE

on non-linear separable multiresolution families using data dependent interpolation. Note that the strong point of these multiresolutions is that they have the ability to consider in their mathematical models the image singularity points. To our knowledge these families have not yet been exploited to map HDR images in LDR images. This paper is organized as follows. Section 2 introduces the basic concepts on the non-linear multiresolution families using dependent data interpolation. A set of operators are then derived. Section 3 evaluates the performance of the derived TMOs. This work is concluded in section 4.

2. Proposed Tone Mapping Operators based on data dependent interpolation

The proposed Image Tone Mapping Operators (TMOs) rely on separable non-linear multiresolution approaches based on data dependent interpolation. The first class exploits the Essentially Non-Oscillatory (ENO) interpolation strategy developed by Harten [9], [10], [11], [12] where Point-Value (PV) mutiresolution family and Cell-Averarage (CA) multiresolution family are considered. The second class concerns the Power-P mutiresolution introduced by Amat [13]. These families have the ability to introduce in their mathematical model the isolated singularities such as edge points in the image thus avoiding the Gibbs phenomenon particularly harmful in tone mapped images.

Before presenting the TMOs, this section introduces the basic concepts of Harten multiresolution. The Point Value (PV), Cell-Average (CA) and Power-P approaches are then derived.

2.1. One-dimensional non-linear Harten multiresolution

This section briefly reviews the non-linear discrete multiresolution strategy developed by Harten. Consider a one-dimensional discrete data set $v^j = (v_k^j)_{k=1,..,N_j}$ defined on the grid $\Gamma^j := (2^{-j}k)_{k=1,..,N_j}$ at resolution level j.

At $j-1$ coarser level, the projection operator, denoted D_j^{j-1}, computes the data set $v^{j-1} = (v_k^{j-1})_{k=1,..,N_{j-1}}$ (with $(N_{j-1} < N_j)$). The prediction operator, denoted P_{j-1}^j, approximates the data set $\hat{v}^j = (\hat{v}_k^j)_{k=1,..,N_j}$ from v^{j-1}. In Harten framework, the projection operator is considered as a non-linear operator. The prediction and projection operators satisfy the following consistency condition:

$$D_j^{j-1} P_{j-1}^j = I_{N_{j-1}}, \tag{1}$$

where $I_{N_{j-1}}$ is the identity operator.

The null space of D_j^{j-1} represents the detail space of dimension $N_j - N_{j-1}$. The prediction error $e^j = v^j - \hat{v}^j$ belongs to the detail space and then expanding it on a basis of that space getting the detail vector $(d_k^{j-1})_{k=1,..,N_j-N_{j-1}}$.

Therefore, one can equivalently write v^j in the form (v^{j-1}, d^{j-1}). Iterating this process, one obtains a multiscale representation of v^J into $(v^0, d^0, d^1, ..., d^{J-1})$.

To adapt the prediction near the singularities of the data, Harten proposed to use ENO interpolation techniques. At resolution level j, the predicted values $(\widehat{v}_{2k+1}^j)_{k=1,..,N_j}$ are approximated by using the values v_k^{j-1} from prediction stencil of length $2M$ defined as:

$$\mathcal{S}(k,r) := \{(k+1-r-M)2^{j-1}, ..., (k-r+M)2^{j-1}\}, \tag{2}$$

where r is an integer in $[-M+1, M-1]$, corresponding to the position of the stencil with respect to k. A polynomial $p_{k,r}$ of degree $2M-1$ is defined to interpolate the value of v on the $\mathcal{S}(k,r)$. Amongst the set of polynomial $p_{k,r}$ with r in $[-M+1, M-1]$, Harten proposed to choose the least oscillatory. To measure the degree of oscillations of such polynomial $p_{k,r}$, the following function is used:

$$C^{j-1}(\mathcal{S}(k,r)) = \sum_{l \in \mathcal{S}_{k,r}} |\Delta v_l^{j-1}|, \tag{3}$$

where $\Delta v_l = v_{l+1} - v_l$.

Therefore the optimal value of r is the solution of the following minimization problem:

$$r^* = \text{argmin}_{-M+1 \le r \le M-1} C^{j-1}(\mathcal{S}(k,r)). \tag{4}$$

2.2. ENO multiresolution family

This section derives 1D ENO predictor operators that will be exploited by our image tone mapping operators.

2.2.1. ENO point-value multiresolution family. In this family, denoted ENO-PV, the discrete vector $v^j := (v_k^j)_{k\in\mathbb{Z}}$ is considered as the point values of the continuous function v on the grid $\Gamma^j := (2^{-j}k)_{k\in\mathbb{Z}}$, i.e. $v_k^j = v(2^{-j}k)$. The operator D_j^{j-1} is considered as the well known downsampling operator i.e. $v_k^{j-1} = v_{2k}^j$. The predictor operator is then defined as data dependent interpolation operator.

By using the values in $v(\lambda)_{\lambda \in S(k,r)}$, the predicted values are then given by:

$$\hat{v}_{2k+1,r}^j = p_{k,r^*}((2k+1)2^{-j}), \tag{5}$$

where the parameter r^* is associated to the polynomial that introduces the least oscillatory around the neighborhood of k according to the cost function given by equation (4).

Now follow the development in [14] and [15]. The prediction values, $\hat{v}_{2k+1,r}^j$ for $r = -1, 0, 1$, are provided for the cubic Lagrange polynomial corresponding to $M = 2$:

$$\begin{cases} \hat{v}_{2k+1,-1}^j = & \frac{1}{16}v_{k-2}^{j-1} - \frac{5}{16}v_{k-1}^{j-1} + \frac{15}{16}v_k^{j-1} + \frac{5}{16}v_{k+1}^{j-1} \\ \hat{v}_{2k+1,0}^j = & -\frac{1}{16}v_{k-1}^{j-1} + \frac{9}{16}v_k^{j-1} + \frac{9}{16}v_{k+1}^{j-1} - \frac{1}{16}v_{k+2}^{j-1} \\ \hat{v}_{2k+1,1}^j = & \frac{5}{16}v_k^{j-1} + \frac{15}{16}v_{k+1}^{j-1} - \frac{5}{16}v_{k+2}^{j-1} + \frac{1}{16}v_{k+3}^{j-1} \end{cases} \tag{6}$$

Note that the prediction $\hat{v}_{2k+1,0}^j$ corresponds to Dubuc-Deslauries interpolatory wavelet.

2.2.2. ENO cell-average multiresolution family. In this family, denoted ENO-CA, the discrete vector $v^j := (v_k^j)_{k\in\mathbb{Z}}$ is considered as the average values of a piecewise continuous function v on the grid $\Gamma_j^k = \{[2^{-j}k, 2^{-j}(k+1)], k \in \mathbb{Z}\}$. The grid here is defined by using the dyadic intervals of the form $I_k^j = [2^{-j}k, 2^{-j}(k+1)]$. The operator D_j^{j-1} becomes in this context the averaging operator:

$$v_k^{j-1} = \frac{1}{2}(v_{2k}^j + v_{2k+1}^j). \tag{7}$$

As in the PV case, the stencil $S(k,r)$ of intervals is given by :

$$\mathcal{S}(k,r) := \{I_{k+1-r-M}^{j-1}, ..., I_{k-r-1+M}^{j-1}\}. \tag{8}$$

The length of the stencil is $2M-1$. A polynomial $p_{k,r}$ of degree $2M-2$ is defined to interpolate the average values on $S(k,r)$. Following the same ENO strategy defined in the PV case, amongst the set of polynomial $p_{k,r}$ with $r = [-M+1, M-1]$, p_{k,r^*} is selected as the least oscillatory polynomial corresponding to r^* deduced from equation (4). The predicted values are then deduced from:

$$\hat{v}_{2k,r}^j = \int_{I_{2k}^j} p_{k,r^*}(t)dt \text{ and } \hat{v}_{2k+1,r}^j = \int_{I_{2k+1}^j} p_{k,r^*}(t)dt. \tag{9}$$

Now follow the development in [14] and [15]. A two order accurate prediction Lagrange interpolation polynomial is used ($M = 2$). Note that from equation (7), only one of the values $\hat{v}_{2k,r}^j$ or $\hat{v}_{2k+1,r}^j$ needs to be computed. The predicted average values, $\hat{v}_{2k+1,r}^j$ for $r = -1, 0, 1$, are then given by:

$$\begin{cases} \hat{v}_{2k+1,-1}^j &= -\frac{1}{8}v_{k-2}^{j-1} + \frac{1}{2}v_{k-1}^{j-1} + \frac{5}{8}v_k^{j-1} \\ \hat{v}_{2k+1,0}^j &= \frac{1}{8}v_{k-1}^{j-1} + v_k^{j-1} - \frac{1}{8}v_{k+1}^{j-1} \\ \hat{v}_{2k+1,1}^j &= \frac{11}{8}v_k^{j-1} - \frac{1}{2}v_{k+1}^{j-1} + \frac{1}{8}v_{k+2}^{j-1} \end{cases} \tag{10}$$

Note that the prediction $\hat{v}_{2k+1,0}^j$ corresponds to the upsampling filter in the biorthogonal wavelet transform $(3,2)$. The biorthogonal scaling function is the box function, i.e. the characteristic function of the interval $[0,1]$.

2.3. Power-P data dependent multiresolution family

In order to emulate the ENO idea in PV context, Amat proposed in [13] to use the Piecewise Polynomial Harmonic (PPH) prediction operator. The PPH operator belongs to a large class of prediction operators, called the Power-P prediction operator. This operator naturally appears as a perturbation of the linear two-point interpolation scheme, since it is defined by:

$$\hat{v}_{2k+1}^j = \frac{v_k^{j-1} + v_{k+1}^{j-1}}{2} - \frac{1}{8}\mathrm{P}\Big(\Delta^2 v_{k+1}^{j-1}, \Delta^2 v_k^{j-1}\Big), \tag{11}$$

with $\mathrm{P}(x,y) = \frac{\mathrm{sgn}(x)+\mathrm{sgn}(y)}{2}\frac{x+y}{2}\left(1 - \left|\frac{x-y}{x+y}\right|^p\right)$, $p \geq 1$. Note that it coincides for $p = 2$ with the harmonic mean and therefore the Power-2 scheme coincides with the PPH scheme. Note also that this prediction is as least first order accurate.

2.4. Tone Mapping Operator using data dependent interpolation

This section presents the proposed approach that maps HDR images to LDR images. The selected operator is based on the extension of the 1D non-linear multiresolution families, described in the previous sections, using classical tensor product approach.

Assume that the HDR image is of size $N \times M$ pixels. Denote T the TMO corresponding to ENO-PV, ENO-CA, PPH or Power-P. It is performed on the logarithmic transformation of the Luma values L_w of the HDR image. Indeed the goal of the logarithm transformation is to take into accounts all the small variations in the scene. Among the various possible logarithmic transformations, the following function is selected:

$$D = \log_b(L_w + \epsilon), \tag{12}$$

where b is the logarithmic basis. ϵ is a positive value added to keep away from cases of logarithmic singularities. The transformed Luma is then decomposed according to the iterated scheme provided by Fig.1. Prediction values are deduced according to one of equations (6), (10) or (11). The process is applied first on the lines and then on the columns of the image.

At a resolution level J, a set of approximation coefficients v^0 and detail coefficients $\{d^0, d^1, d^2, ..., d^{J-1}\}$ are obtained. These coefficients are scaled as follows: $\beta \times v^0$ with $0 \leq \beta \leq 1$; and $\gamma \times \{d^0, d^1, d^2, ..., d^{J-1}\}$ with $0 \leq \gamma \leq 1$.

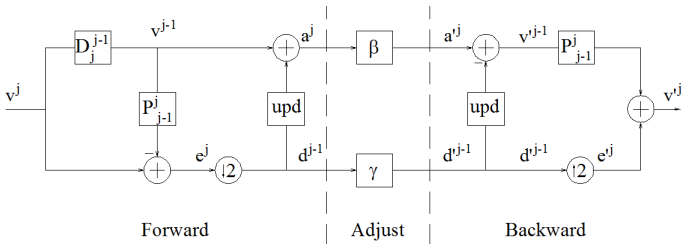

Figure 1. Forward and backward steps at a given level j.

3. Simulation results

This section compares the quality of the tone mapped images using the mutiresolution families described in the previous sections. The tone-mapped image quality is measured with the TMQI (Tone-Mapped image Quality Index) metric developed in [16]. This metric evaluates the LDR image using the original HDR image. Note that TMQI measure is upper-bounded by 1. Simulations have been conducted under Matlab environnement using the HDR Toolbox [1] with its test HDR images "Bottle Small", "Office", "Oxford Church" and "Atrium Night". The different parameters are chosen so as to give the best results in terms of TMQI metric in all methods.

Four TMO operators namely ENO-PV, ENO-CA, PPH (Power-2) and Power-P (with $P = 4$) are used with the following parameters $\beta = 0.3$, $\gamma = 0.7$, J=2, upd=0, $b = e$. They are compared to :
- Fattal [8] using WCDF and RBW methods with the following parameters $\alpha = 0.8$, $\beta = 0.3$, $\gamma = 0.8$, J=2, upd=0;
- Drago [3], Reinhard [4], Ward [5], Durand [2] with the default parameters as given in the HDR Toolbox and Duan [7] using $\beta = 0.3$.

Table 1 provides the tone mapped images TMQI according to these different methods. The performance of the non-linear multiresolution families is competitive to Fattal [8]. Also note that our solutions are less costly in terms of computations than WCDF requiring the computation and the storage of weight coefficients for the reconstruction step.

The tone mapped HDR "Bottle Small" using RBW, WCDF, ENO-CA, ENO-PV, Power-4, PPH operators is respectively given by Fig.2, Fig.3, Fig.4, Fig.5, Fig.6 and Fig.7. These images have a similar visual quality.

Although TMQI of ENO-PV (0.89) is slightly lower than Fattal (0.94) for "Atrium Night" HDR image, some visual details are best rendered by our solution. The luminance of "Atrium Night" HDR tone mapped image is represented on Fig. 8a where the red rectangle frames a specific area. This area is shown in Fig. 8b, Fig. 8c, Fig. 8d, Fig. 8e, Fig. 8f, Fig. 8g as close-ups of the six tone mapped images using RBW, WCDF, ENO-CA, ENO-PV, PPH, Power-4. It can be seen that the horizontal edge of the staircase step is better rendered with non-linear multiresolution families using dependent data interpolation. We can observe that horizontal and vertical edges of all tone mapped images are well rendered. This is related to the separability of the approach. In our future work, we will investigate the non-separable approach as suggested in [14] and [15] to further improve the LDR image rendering.

TABLE 1. TONE MAPPED IMAGE QUALITY INDEX (TMQI)

TM methods	Bottle Small	Small Office	Oxford Church	Atrium Night
Drago [3]	0.801	0.801	0.814	0.799
Reinhard [4]	0.807	0.826	0.789	0.801
Ward [5]	0.783	0.775	0.817	0.797
Durand [2]	0.892	0.825	0.814	0.929
Duan [7]	0.915	0.955	0.986	0.964
Fattal WCDF [8]	0.969	0.920	0.914	0.941
Fattal RBW [8]	0.972	0.920	0.916	0.944
ENO-CA	0.968	0.889	0.930	0.945
ENO-PV	0.960	0.875	0.917	0.891
PPH	0.964	0.873	0.916	0.921
Power-4	0.967	0.871	0.918	0.917

Figure 2. Fattal's RBW ($\alpha = 0.8$, $\beta = 0.3$, $\gamma = 0.8$, J=2, upd=0).

Figure 3. Fattal's WCDF ($\alpha = 0.8$, $\beta = 0.3$, $\gamma = 0.8$, J=2, upd=0).

Figure 4. ENO-CA ($\beta = 0.3$, $\gamma = 0.7$, J=2, upd=0, $b = e$).

4. Conclusion

This paper evaluated the performance of the image tone mapping operators derived from the separable non-linear multiresolution families. These families, based on data dependent interpolation, include in their mathematical model the singularity points of the HDR image. The Gibbs phenomenon that affects the visual quality of the tone mapped image is then reduced. Moreover vertical and horizontal edges are well rendered. Simulations results are competitive to the image tone mapping operators available in the state of the art. To further improve the LDR image rendering we plan to investigate the non-separable approach as suggested in [14] and [15].

Figure 5. ENO-PV ($\beta = 0.3$, $\gamma = 0.7$, J=2, upd=0, $b = e$).

Figure 6. PPH ($\beta = 0.3$, $\gamma = 0.7$, J=2, upd=0, $b = e$).

Figure 7. Power-4 ($\beta = 0.3$, $\gamma = 0.7$, J=2, upd=0, $b = e$).

(a) Atrium Night (LDR luminance)

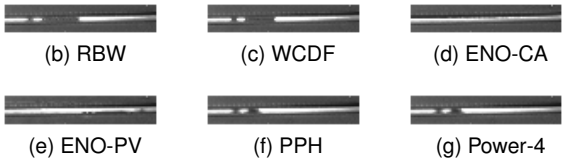

Figure 8. Close-up of the tone mapped image luminance using RWB, WCDF, ENO-CA, ENO-PV, PPH and Power-4.

References

[1] Banterle, F., Artusi, A., Debattista, K., and Chalmers, A., *Advanced High Dynamic Range Imaging*, Theory and Practice AK Peters (now CRC Press), ISBN: 978-156881-719-4 (2011).

[2] Durand, F., and Dorsey, J., *Fast bilateral filtering for the display of high-dynamic-range images*, ACM Transactions on Graphics (TOG) - Proceedings of ACM SIGGRAPH 21 (2002), 257-266.

[3] Drago, F., Myszkowski, K., Annen, T., and Chiba, N., *Adaptive logarithmic mapping for displaying high contrast scenes*, Computer Graphics Forum 22 (2003), 419-426.

[4] Reinhard, E., and Devlin, K., *Dynamic range reduction inspired by photoreceptor physiology*, IEEE Transactions on Visualization and Computer Graphics 11 (2005), 13-24.

[5] Ward, G., Rushmeier, H., and Piatko, C., *A visibility matching tone reproduction operator for high dynamic range scenes*, IEEE Transactions on Visualization and Computer Graphics 3 (1997), 291-306.

[6] Li, Y., Sharan, L., and Adelson, E., *Compressing and companding high dynamic range images with subband architectures*, ACM Transaction on Graphics 24(3), 836-844 (2005).

[7] Duan, J., Bressan, M., Dance, C., and Qiu, G., *Tone-mapping high dynamic range images by novel histogram adjustment*, Pattern Recognition, vol. 43, 5 (2010), 1847-1862.

[8] Fattal, R., *Edge-Avoiding Wavelets and their Applications*, ACM Trans. Graph (2009).

[9] Harten, A., *Multiresolution representation of data: a general framework*. SIAM J. Numerical Analysis. 33, 3 (1996), 1205-1256.

[10] Aràndiga, F., and Donat, R., *Nonlinear multiscale decompositions: The approach of A.Harten*, Numerical Algorithms, 23 (2000), 175-216.

[11] Harten, A., Engquist, B., Osher, S., and Chakravarthy, S., *Uniformly high order accurate essentially non-oscillatory schemes III*, Journal of Computer, Physics 71, (1987), 231-303.

[12] Amat, S., Aràndiga, F., Cohen, A., Donat, R., Garcia, G., and Oehsen, M.V., *Data compression with ENO schemes : A case study*, Applied and Computational Harmonic Analysis, vol. 11, 2 (2001), 273-288.

[13] Amat, S., Donat, R., Liandrat, J. and Trillo; J.C. *A fully adaptive PPH multiresolution scheme for image processing*, Mathematical and Computer Modelling (2006).

[14] Matei, B. and Meignen, S. *Nonlinear Cell-Average Multiscale Signal Representations: Application to Signal Denoising*, Signal Processing, vol. 92, no. 11, pp. 2738-2746, 2012.

[15] Matei, B. and Meignen, S. *Nonlinear and Nonseparable Bidimensional Multiscale Representation Based on Cell-Average Representation*,IEEE Transactions on Image Processing, 2015.

[16] Yeganeh, H. and Wang, Z., *Objective quality assessment of tone-mapped images*, IEEE Trans on Image Processing, vol. 22, pp. 657-667 (February 2013).